Supporting Information

Radical Pair Reaction Schemes.

A number of variants on the basic reaction scheme in Fig. 1 are possible. A few are discussed briefly here.

Initial triplet state.

The photoexcited state B* could be a triplet (formed by intersystem crossing from the photoexcited singlet state) so that the initial radical pair state would be $^{T}[A^{\bullet+}B^{\bullet-}]$ rather than $^{S}[A^{\bullet+}B^{\bullet-}]$. The scheme in Fig. 1 would then become as shown in Fig. S1.

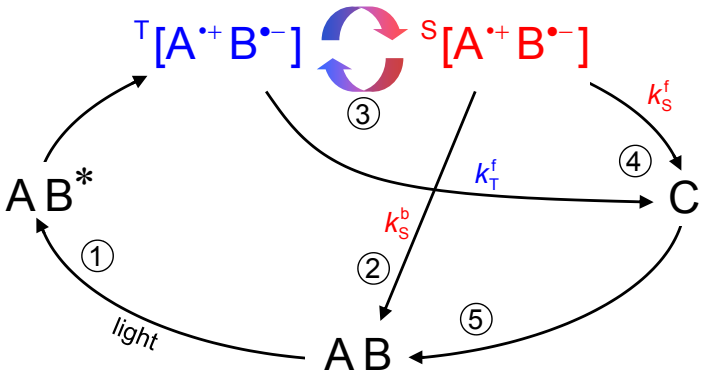

Fig. S1. A simple reaction scheme that could form the basis of a compass magnetoreceptor. This version of Fig. 1 is appropriate when the radical pair is initially formed in a triplet instead of a singlet state. Details are given in the *Perspective*.

Here, in contrast to the initial singlet case (Fig. 1), if the external magnetic field had the effect of reducing the efficiency of S ↔ T interconversion, more C would be formed because fewer radical pairs would reach the singlet state and there would consequently be less recombination to A B via step 2.

Sequential electron transfers.

The formation of the radical pair need not be a single-step reaction. It could be a sequence of fast electron transfers, as occurs in photosynthetic reaction center proteins. A general reaction scheme for a series of 3 consecutive radical pairs (RP_1, RP_2 and RP_3) is shown in Fig. S2 (1).

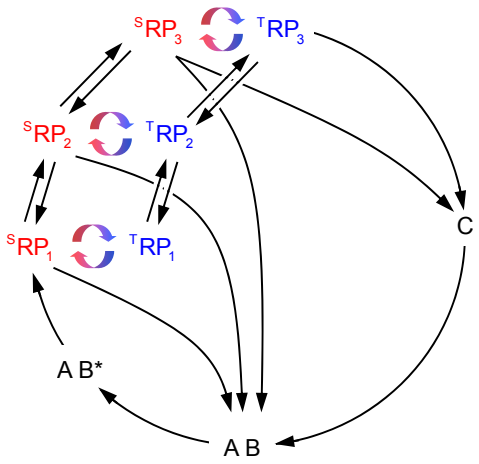

Fig. S2. A simple reaction scheme that could form the basis of a compass magnetoreceptor. This version of Fig. 1 includes a series of 3 consecutive radical pairs formed by sequential electron transfers. RP_1, RP_2, and RP_3 are primary, secondary, and tertiary radical pairs.

In principle, there could be S ↔ T interconversion in, and hence magnetic field effects from, all 3 radical pairs. It seems likely that more efficient magnetoreception would result if only RP_3 were magnetically sensitive. This would be the case either if the first 2 electron transfer steps ($RP_1 \rightarrow RP_2$ and $RP_2 \rightarrow RP_3$) are fast compared with S ↔ T interconversion or if the exchange and/or dipolar couplings in RP_1 and RP_2 are large enough to block S ↔ T interconversion (2).

The first and second electron transfers need not be reversible. Nor is recombination of $^{S}RP_1$ or $^{S}RP_2$ to the ground state a requirement. A simplified but still viable version of the above scheme would therefore be as shown in Fig. S3.

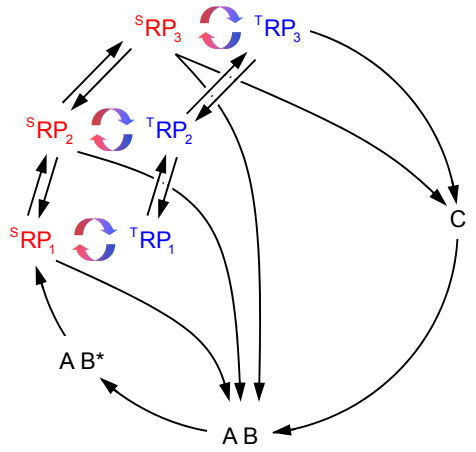

Fig. S3. A simple reaction scheme that could form the basis of a compass magnetoreceptor. In this version of Fig. S2, RP_2 and RP_3 are formed irreversibly, and RP_1 and RP_2 do not recombine to the ground state.

This is essentially identical to Fig. 1, the only difference being the details of the effectively instantaneous formation of the magnetically sensitive radical pair (RP_3).

Signaling state.

It seems likely that $[A^{\bullet+}B^{\bullet-}]$, with a probable lifetime of ~1 μs, is too short-lived to be the signaling state, hence the requirement to form a much longer-lived species C. Fig. 1 contains no information on the types of reactions that might lead to the formation of C or its subsequent conversion back to A B. Here, we offer a few possibilities.

One possibility is that C could be a longer lived radical pair, which need not be magnetically sensitive, formed, for example, by one or more subsequent electron transfer steps involving additional donors or acceptors:

$$D + A^{\bullet+}B^{\bullet-} \rightarrow D^{\bullet+}A\,B^{\bullet-} \quad \textit{or} \quad A^{\bullet+}B^{\bullet-} + E \rightarrow A^{\bullet+}\,B\,E^{\bullet-}$$

Alternatively, a longer-lived radical pair state could result from (de)protonation or chemical reaction of one or both of the radicals (3). Note that if such a process occurred on a time scale that was fast compared with S ↔ T interconversion, the net effect would simply be a change in the identity of the magnetically sensitive radical pair (e.g., $RP_1 \rightarrow RP_2$ and $RP_2 \rightarrow RP_3$ in Fig. S3).

C does not have to be a radical pair. One or both of $A^{\bullet+}$ and $B^{\bullet-}$ could be converted into nonradical species, e.g., via oxidation or reduction steps:

$$F_{red} + A^{\bullet+}B^{\bullet-} \rightarrow F_{ox} + A\,B^{\bullet-} \quad \textit{or} \quad G_{ox} + A^{\bullet+}B^{\bullet-} \rightarrow G_{red} + A^{\bullet+}\,B\,,$$

where F_{red} and G_{ox} are reducing and oxidising agents, respectively. Some combination of these processes would also be possible.

None of the above reactions is spin selective and so all would have $k_S^f = k_T^f$.

Alternatively, C could be formed by a spin-selective reaction, e.g., back electron transfer from the triplet state of the radical pair to form the excited triplet state of A or

B (as happens in photosynthetic reaction centers when forward electron transfer is blocked):

$$^{T}[A^{\bullet+}B^{\bullet-}] \rightarrow {}^{T}AB \quad or \quad {}^{T}[A^{\bullet+}B^{\bullet-}] \rightarrow A\,{}^{T}B$$

In this case $k_S^f = 0$.

Clearly, the method of conversion of C back to A B is dependent on the identity of C. If it is a long-lived radical pair, then back electron transfer would serve the purpose. If it is $AB^{\bullet-}$ or $A^{\bullet+}B$ (see above), then a further oxidation or reduction step would be required. If C is a triplet state, then intersystem crossing would return it to the ground state.

The magnetically sensitive radical pair could be formed by hydrogen atom transfer (e.g., $AH\text{-}B \rightarrow [A^{\bullet}\,BH^{\bullet}]$) or homolytic bond cleavage (e.g., $A\text{-}B \rightarrow [A^{\bullet}\,B^{\bullet}]$), but such reactions are much less likely than electron transfer to produce radicals with a suitable separation and appropriate kinetics (see below).

Biological Radical Pair Reactions.

As described in the *Perspective*, by far the most intensively studied biological radical pairs occur in the initial steps of photosynthetic energy conversion. Other biological radical pair processes are less well established and are briefly mentioned here.

Magnetic field effects on enzymatic reactions of ethanolamine ammonia lyase (EAL) (4-6) and horseradish peroxidase (HRP) (7-10) have been reported and related effects have been found for the peroxidase-oxidase oscillator (11-14). However, independent attempts to replicate the original observations from Grissom's laboratory on both HRP and EAL have been unsuccessful (15, 16). Other biomolecules in which spin-correlated radical pairs have been reported include melanin (17), a mutant phototropin LOV2 domain (18, 19), and several phosphorylating enzymes (20-22). One of the latter—phosphocreatine kinase—apparently shows a magnetic field response (20). The occurrence of photoinduced spin-correlated radical pairs in photolyase and cryptochrome is summarized in the *Perspective*.

Radical pairs showing a variety of spin-chemical effects can routinely be generated by intermolecular reactions of photoexcited dye molecules (e.g., flavins and other aza-aromatics) with solvent-exposed aromatic amino acid residues in proteins (23-28). Such freely diffusing radical pairs are less likely to be sensitive to the presence and direction of a weak applied magnetic field than those formed by intraprotein electron transfer.

Details of Simulations Presented in Fig. 2.

The radical pair for which the simulations in Fig. 2 were performed contains a single magnetic nucleus with spin quantum number $I = ½$ and a 500-μT isotropic hyperfine coupling and is initially in a pure singlet state at time $t = 0$. The kinetics are first order, there are no interradical interactions, and spin relaxation is ignored. The applied magnetic field strength is zero (Fig. 2*A*) or 50 μT (Fig. 2*B*). The green traces show the time dependence of the fraction of radical pairs that exist in the triplet state, $p_T(t)$, in the absence of chemical reactivity (i.e., $k_S^f = k_S^b = k_T^f = 0$). The red and blue traces represent, respectively, $p_T(t)$ and the yield of the product (species C in Fig. 1) when reaction steps are included ($k_S^f = 0$; $k = k_S^b = k_T^f = 10^6\ s^{-1}$). See Fig. 1 for the definitions of the rate constants.

The time-dependence of $p_T(t)$ and the yield of C are given by (29):

$$p_T(t) = e^{-kt}\left[\frac{5}{8} - \frac{1}{8}\frac{\omega^2}{\Omega^2} - \frac{1}{8}\frac{a^2}{\Omega^2}\cos\Omega t - \frac{1}{8}\left[1-\frac{\omega}{\Omega}\right]\cos\tfrac{1}{2}(a+\omega+\Omega)t - \frac{1}{8}\left[1-\frac{\omega}{\Omega}\right]\cos\tfrac{1}{2}(a-\omega-\Omega)t - \frac{1}{8}\left[1+\frac{\omega}{\Omega}\right]\cos\tfrac{1}{2}(a-\omega+\Omega)t - \frac{1}{8}\left[1+\frac{\omega}{\Omega}\right]\cos\tfrac{1}{2}(a+\omega-\Omega)t\right]$$

$$[C]_t = k\int_0^t p_T(t')\,dt'$$

where a is the isotropic hyperfine coupling constant, ω is the electron Zeeman interaction, both expressed as angular frequencies, and $\Omega = \sqrt{a^2+\omega^2}$.

Details of Simulations Presented in Fig. 3.

The simulations shown in Fig. 3 were performed as described in refs. 2 and 30 using the reaction scheme of Fig. 1 with $k_{\mathrm{S}}^{\mathrm{f}} = 0$; $k_{\mathrm{S}}^{\mathrm{b}} = k_{\mathrm{T}}^{\mathrm{f}} = k = 2\times10^{5}\ \mathrm{s}^{-1}$ and a 50-μT magnetic field. The radical pair is initially in a pure singlet state at time t = 0, the kinetics are first order, there are no interradical interactions, and spin relaxation is ignored. The triplet yield is defined as $\Phi_{\mathrm{T}}(\theta,\phi) = [\mathrm{C}]_{\infty}$ where $[\mathrm{C}]_t$ is the yield of species C at time t ($0 \le [\mathrm{C}]_t \le 1$), and the polar angles θ and ϕ define the direction of the magnetic field with respect to the frame of the radical pair. The polar plots (upper row) show the anisotropic parts of the triplet yield, $\Phi_{\mathrm{T}}^{\mathrm{aniso}} = \Phi_{\mathrm{T}} - \langle\Phi_{\mathrm{T}}\rangle$, where $\langle\Phi_{\mathrm{T}}\rangle$ is the spherical average of Φ_{T}. See ref. 31 for further examples. The polar plots are constructed by plotting a point, for each direction of the applied magnetic field, at a distance from the origin proportional to the absolute value of $\Phi_{\mathrm{T}}^{\mathrm{aniso}}$. The surface color is a spectrum in which the maximum (i.e., most positive) $\Phi_{\mathrm{T}}^{\mathrm{aniso}}$ is red and the minimum (i.e., most negative) $\Phi_{\mathrm{T}}^{\mathrm{aniso}}$ is blue.

The signal (or "visual") modulation patterns (lower row) were calculated from $\Phi_{\mathrm{T}}^{\mathrm{aniso}}$ using a simple model developed by Ritz *et al.* (32) to illustrate how a field-sensitive reaction in the visual pathway might allow a bird to perceive the geomagnetic field. Despite the naïveté of this model, it serves to show how the radical pair mechanism could in principle deliver intelligible compass information. Furthermore, it gives some sense of the quality of the information that might arise from a particular choice of radical pair and other model parameters.

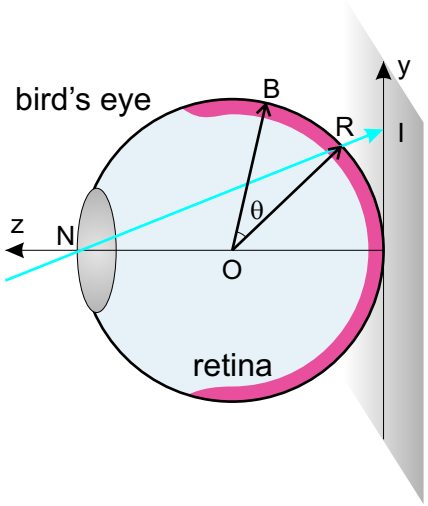

Fig. S4. Cross-section through a bird's eye, modeled as a unit sphere. Following Ritz *et al.* (32), this model is used to calculate signal modulation patterns.

Following Ritz *et al.* (32), we model the bird's eye as a unit sphere centered at the origin O, as shown in Fig. S4. Light travels from the scene under observation through the pupil (modeled as a pinhole at point N) and strikes the retina. One particular ray of light, drawn for illustration, intersects the retina at point R. We envisage that the light is perceived by the bird as forming an image in the *xy*-plane at point I. Hence, a rectangular object will create a rectangular perceived image in the plane containing I. Thus, the eye is assumed to function as a pinhole camera. The points N, O, R and I all lie in the plane of the paper. B may be at any point on the surface of the eyeball, i.e., B is not constrained to lie in the plane NOR.

We suppose next that light incident on the retina creates radical pairs in an initial singlet state which react according to the radical pair mechanism. Only the product formed from the triplet state of the radical pair (the "triplet product") goes on ultimately to trigger an impulse in the optic nerve. In other words, for any point R on the retina or, equivalently, for any point I in the perceived image

$$\textit{Perceived light intensity} = \textit{Triplet yield at the retina} \times \textit{True light intensity}$$

The triplet yield depends on the relative orientation of the photoinduced radical pair and the geomagnetic field, which varies across the curved surface of the retina. Hence, the geomagnetic field modulates the contrast of the perceived image by different

amounts at different points in the field of vision. We wish to calculate a picture showing that modulation throughout the field of vision.

To continue, we make a further assumption concerning the arrangement of radical pairs with respect to the retina. We assume that every radical pair has a well-defined orientation with respect to the retinal surface normal vector $\overrightarrow{\mathrm{OR}}$ but that they are otherwise randomly oriented. This seems reasonable given that histological images of the retina show long, thin light-receptor cells whose axis points towards the center of the eye but which are not otherwise oriented. Notice that this assumption means that the signal modulation patterns for Fig. 3 *C* and *D* are identical.

The geomagnetic field is directed along the vector $\overrightarrow{\mathrm{OB}}$. The singlet yield for a radical pair at the point R is a function of the polar angle θ between $\overrightarrow{\mathrm{OR}}$ and $\overrightarrow{\mathrm{OB}}$ which is well defined, and the azimuthal angle ϕ (defined as a rotation about the vector $\overrightarrow{\mathrm{OR}}$) which is randomly distributed between 0 and 2π. To take account of this uniaxial alignment, we calculate an average axial triplet yield

$$\tilde{\Phi}_{\mathrm{T}}(\theta) = \frac{1}{2\pi}\int_0^{2\pi} \Phi_{\mathrm{T}}(\theta,\phi)\, d\phi$$

Now, to determine the signal modulation pattern for each point I with Cartesian coordinates (x, y) in the field of vision, it remains only to relate those coordinates to the polar angle θ. To do this, we must first determine the position of the point R using the fact that the line NRI intersects the shaded plane at point I.

The position vector $\mathbf{r}_I$ satisfies the equation of a plane

$$\mathbf{r}_I \bullet \mathbf{k} = -1$$

where $\mathbf{i}$, $\mathbf{j}$ and $\mathbf{k}$ are unit vectors along the *x*-, *y*- and *z*-axes. Meanwhile the position vector $\mathbf{r}_{NI}$ of any point on the line NRI satisfies the equation of a line

$$\mathbf{r}_{NI} = \alpha(\mathbf{r}_R - \mathbf{k}) + \mathbf{k}$$

in which α is an arbitrary real number.

Since the point I lies both on the line NRI and in the shaded plane, $\mathbf{r}_I$ satisfies both equations and hence

$$\begin{aligned}\left(\alpha\left(\mathbf{r}_R-\mathbf{k}\right)+\mathbf{k}\right)\bullet\mathbf{k}&=-1\\ \alpha\left(\mathbf{r}_R\bullet\mathbf{k}-1\right)&=-2\\ \Rightarrow\alpha&=\frac{2}{1-\mathbf{r}_R\bullet\mathbf{k}}\end{aligned}$$

and thus

$$\mathbf{r}_I=\frac{2\left(\mathbf{r}_R-\mathbf{k}\right)}{1-\mathbf{r}_R\bullet\mathbf{k}}+\mathbf{k}$$

If we write $\mathbf{r}_R$ in spherical polar coordinates,

$$\mathbf{r}_R=\sin\theta_R\cos\phi_R\mathbf{i}+\sin\theta_R\sin\phi_R\mathbf{j}+\cos\theta_R\mathbf{k}$$

then

$$x_I=\frac{2\sin\theta_R\cos\phi_R}{1-\cos\theta_R}\quad\text{and}\quad y_I=\frac{2\sin\theta_R\sin\phi_R}{1-\cos\theta_R}$$

which rearrange to give

$$\tan\phi_R=\frac{y_I}{x_I}\Rightarrow\cos\phi_R=\frac{x_I}{r_I}\quad\text{and}\quad\sin\phi_R=\frac{y_I}{r_I}$$

and

$$\cos\theta_R=\frac{r_I^2-4}{r_I^2+4}\quad\text{and}\quad\sin\theta_R=\frac{4r_I}{r_I^2+4}$$

where $r_I^2\equiv x_I^2+y_I^2$.

Having found the position vector $\mathbf{r}_R$ of the point R, the angle θ is given by the dot product

$$\begin{aligned}\cos\theta &= \mathbf{r}_R \bullet \mathbf{r}_B \\ &= \left(\frac{4r_I}{r_I^2+4}\right)\left(\frac{x_I}{r_I}x_B + \frac{y_I}{r_I}y_B\right) + \left(\frac{r_I^2-4}{r_I^2+4}\right)(z_B) \\ &= \left[x_I x_B + y_I y_B + \left(\left(\frac{r_I}{2}\right)^2 - 1\right)z_B\right] \Big/ \left[\left(\frac{r_I}{2}\right)^2 + 1\right]\end{aligned}$$

for a magnetic field $\mathbf{r}_B = x_B\mathbf{i} + y_B\mathbf{j} + z_B\mathbf{k}$.

This last equation allows us to construct an image, calculating the intensity modulations at every point from the magnetic field vector $\mathbf{r}_B$ and the average axial triplet yield $\tilde{\Phi}_{\mathrm{T}}(\theta)$. Such images are shown in Fig. 3 and in Fig. S6. The field of view in these images is ±31° in the horizontal and vertical directions.

Calculations were performed for the following spin systems:

(A) One radical contains no magnetic nuclei, the second contains 2 I = 1 nuclei representing N5 and N10 in the flavin radical anion $FAD^{\bullet-}$. The hyperfine tensors for these nuclei were calculated by Ilya Kuprov for a model compound using Gaussian03 with a ROB3LYP/6-311++g(2d,2p) level of theory for the geometry optimisation and UB3LYP/EPR-III for the hyperfine calculation. They are (in millitesla):

$$A_{N5} = \begin{pmatrix} -0.098853 & 0.003884 & 0 \\ 0.003884 & -0.088056 & 0 \\ 0 & 0 & 1.7569 \end{pmatrix}$$

$$A_{N10} = \begin{pmatrix} -0.018967 & -0.004841 & 0 \\ -0.004841 & -0.019578 & 0 \\ 0 & 0 & 0.60458 \end{pmatrix}$$

(B) This is the same as case (A), except now the first radical is based on a model of the tyrosyl radical and contains 5 hydrogen (I = ½) nuclei. Calculations were performed using Gaussian03 with a ROB3LYP/6-31+g(3d,3p) geometry, with

PCM solvation in water and with UB3LYP/EPR-III theory for the hyperfine calculation. The hyperfine tensors (in millitesla) for the first radical are:

$$A_{H7} = \begin{pmatrix} -0.831109 & -0.001023 & 0.235725 \\ -0.001023 & -0.693348 & 0.002233 \\ 0.235725 & 0.002233 & -0.337353 \end{pmatrix}$$

$$A_{H10} = \begin{pmatrix} -0.836629 & -0.001018 & -0.238049 \\ -0.001018 & -0.697746 & -0.002223 \\ -0.238049 & -0.002223 & -0.340778 \end{pmatrix}$$

$$A_{H13} = \begin{pmatrix} 2.6742 & -0.094273 & -0.002583 \\ -0.094273 & 2.591505 & 0.003779 \\ -0.002583 & 0.003779 & 2.476992 \end{pmatrix}$$

$$A_{H14} = \begin{pmatrix} 0.762199 & 0.032411 & -0.079955 \\ 0.032411 & 0.604102 & -0.012137 \\ -0.079955 & -0.012137 & 0.664062 \end{pmatrix}$$

$$A_{H15} = \begin{pmatrix} 0.666082 & 0.029032 & 0.080419 \\ 0.029032 & 0.509596 & 0.009021 \\ 0.080419 & 0.009021 & 0.568135 \end{pmatrix}$$

The hyperfine tensors for N5 and N10 in the second radical were as above.

(C) This spin system is chosen arbitrarily to illustrate the more complicated yield anisotropy patterns that sometimes arise. One radical contains a single hydrogen (I = ½) with hyperfine tensor (in millitesla)

$$A_{A1} = \begin{pmatrix} 0.013125 & 0.004575 & 0.017075 \\ 0.004575 & 0.00183 & 0.007061 \\ 0.017075 & 0.007061 & 0.022544 \end{pmatrix}$$

the other has 2 nitrogen (I = 1) with hyperfine tensors (in millitesla)

$$A_{B1} = \begin{pmatrix} -0.000683 & -0.007598 & 0.004231 \\ -0.007598 & 0.032391 & -0.01847 \\ 0.004231 & -0.01847 & 0.007541 \end{pmatrix}$$

$$A_{B2} = \begin{pmatrix} 0.000020 & -0.002641 & 0.001299 \\ -0.002641 & 0.011213 & -0.006219 \\ 0.001299 & -0.006219 & 0.002916 \end{pmatrix}$$

(D) This final calculation was made using the same spin system as in (C) but for radical pairs that were rotationally disordered around the z-axis. This is equivalent to averaging the product yield around the z-axis.

Dependence of Reaction Yield on Radical Pair Lifetime.

An estimate of the effect of a weak magnetic field on the yield of a radical pair reaction may be obtained analytically for a pair containing a single spin-½ nucleus, assuming the (isotropic) hyperfine coupling constant a is much larger than both the intensity of the applied magnetic field ($\gamma_e B_0$) and the recombination rate constant k (Fig. 1 reaction scheme with $k_S^f = 0$; $k_S^b = k_T^f = k$). The fractional change in the product yield relative to zero field is (29):

$$\left| \frac{\Phi_S(B_0) - \Phi_S(0)}{\Phi_S(0)} \right| = \left[2.50 \; + \; 3.23 \times 10^8 (B_0 / \mu\mathrm{T} \times \tau / \mathrm{ns})^{-2} \right]^{-1}$$

where τ = $1/k$ is the radical pair lifetime and $\Phi_S(B_0)$ is the singlet yield ($\Phi_S(B_0) = 1 - \Phi_T(B_0) = 1 - [\mathrm{C}]_\infty$) in the presence of a field of intensity B_0.

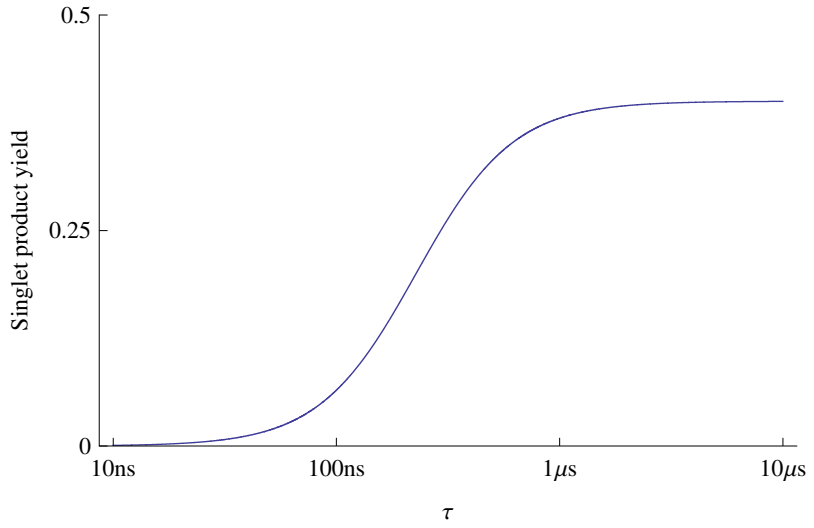

Fig. S5. Fractional change in the isotropic reaction yield of a simple radical pair as a function of the radical pair lifetime τ in a magnetic field of 50 μT.

The dependence of the fractional change in the product yield is shown in Fig. S5 for B_0 = 50 μT. Although this calculation has been performed for a very simple radical pair, without anisotropic hyperfine interactions, it is reasonable to expect something similar in more realistic cases. The conclusion is that there is little to be gained, in terms of increased product yield or magnetic sensitivity, by having a lifetime longer than ~1 μs when the external magnetic field is ~50 μT.

Dependence of Electron Transfer Rates on Donor-Acceptor Separation.

The rate constant, k_{ET}, for electron transfer in a protein is related approximately to the donor-acceptor edge-to-edge separation r_{e} via Marcus theory (33):

$$\log_{10}(k_{\mathrm{ET}}/\mathrm{s}^{-1}) = 15 - 6r_{\mathrm{e}}/\mathrm{nm} - 3.1\left[\frac{(\Delta_{\mathrm{r}}G^{\ominus} + \lambda)^2}{\lambda}\right]/\mathrm{eV}$$

For a given r_{e}, the optimum electron transfer rate occurs when the reaction Gibbs energy matches the reorganization energy, $\Delta_{\mathrm{r}}G^{\ominus} = -\lambda$, i.e.,

$$\log_{10}(k_{\mathrm{ET}}/\mathrm{s}^{-1}) \leq 15 - 6r_{\mathrm{e}}/\mathrm{nm}$$

On the basis that the lifetime of the radical pair should be ~1 μs (to allow enough time for S ↔ T interconversion, but not enough for significant spin relaxation), we have $k_{ET} \approx 10^6$ s^{-1} and hence $r_e \leq 1.5$ nm for the magnetically sensitive radical pair.

There are other kinetic constraints that probably need to be satisfied for efficient magnetoreception. It seems likely that the magnetically sensitive radical pair, whether produced directly from a photoexcited state (as in Fig. 1) or via photoinitiated sequential electron transfers (1), needs to be formed rapidly in order to compete with other processes that may deactivate the precursor species (e.g., fluorescence and internal conversion) and to maximize the spin correlation in the terminal, magnetosensitive radical pair in an electron transfer chain. To achieve a high radical pair quantum yield, a plausible lower limit on the forward electron transfer rate would be ~10^9 s^{-1}, implying $r_e \leq 1.0$ nm for each of the electron donor-acceptor pairs involved in the formation of the magnetoreceptive radical pair.

Quenching of Magnetic Field Effects by Strong Radical-Radical Interactions. Experimentally, there is ample evidence that large radical-radical interactions block S ↔ T interconversion and so remove the possibility that reaction yields can be altered by weak applied magnetic fields. For example, some of the smaller molecular dyads and triads developed as models of photosynthetic electron transport have large exchange interactions and are insensitive to weak fields (34-36). In addition, several flavin-based blue-light photoreceptors—phototropin LOV (light, oxygen, and voltage sensing) domains and BLUF (blue light sensing using FAD) domains—appear to have radical pair intermediates whose inter-radical separations are too small ($r_e < 0.5$ nm) to be compatible with significant magnetic sensitivity (37-40). For similar reasons, the DNA repair activity of photolyase is unlikely to respond to applied magnetic fields (41).

Finally, hydrogen atom transfer and homolytic bond cleavage reactions are short range and therefore unlikely to produce radical pairs with sufficiently small exchange and dipolar interactions.

Disorder and Motion.

Examples of slowly relaxing spin-correlated radical pairs.

Experimental evidence for slow relaxation of spin-correlated radical pairs in ~50-μT fields at physiological temperatures is scarce. Most EPR measurements are performed in magnetic fields of at least 300 mT, often at cryogenic temperatures, and extrapolation to weaker fields and higher temperatures is not straightforward. However, examples of spin correlation persisting for more than 1 μs at room temperature do exist, e.g., 3 different radical pairs in plant photosystems (42-44). The observation of electron spin-polarized EPR signals from photosynthetic radical pairs at room temperature also shows that molecular tumbling can be slow enough (>1 μs) that anisotropic magnetic interactions as weak as ~50 μT are not rotationally averaged (42-44).

Constraints on types of radicals that could have sufficiently slow spin relaxation.

Although the need to preserve spin correlation and hyperfine anisotropy imposes significant restrictions on the dynamics of the radical pair, it does not substantially narrow the search for the identity of the magnetoreceptor. However, a few possibilities can, probably, be excluded. Species with significant spin density on paramagnetic transition metal atoms, often relax very efficiently (45) and are not the most obvious candidates for a magnetoreceptor. High-symmetry radicals with orbitally degenerate ground states may also have very short relaxation times. For example, with 2 possible exceptions (46, 47), no spin chemistry phenomena seem to have been reported for radical pairs containing hydroxyl $OH^{\bullet}$, superoxide $O_2^{\bullet-}$ or nitric oxide $NO^{\bullet}$. Electron spin-correlation in radical pairs can also be efficiently relaxed by nearby paramagnetic centers, as occurs for the high-spin non-heme Fe^{2+} in bacterial photosynthetic reaction centers (48).

Translational motion in radical pairs.

In principle, a compass magnetoreceptor could be constructed around a radical pair in which one radical is able to move, provided the other is fixed and ordered and had suitably anisotropic hyperfine interactions. Allowing one radical freedom to separate from its partner might circumvent the problems associated with excessive interradical spin-spin interactions provided the mobile radical had a high probability of

re-encountering its partner on an appropriate timescale. Possible means of restricting the diffusive separation of the radicals include viscous solvents, spatially constrained diffusion (e.g., inside a micelle or, conceivably, a membrane), strong attractive Coulomb forces between charged radicals, or, possibly, linking the radical centers by a flexible molecular chain (as in a biradical) (29, 49). However, the mobile radical would need to undergo very fast rotational motion in order to relax sufficiently slowly, a condition that may not be compatible with the need to restrict the translational motion. It therefore seems improbable but not impossible that a radical pair magnetoreceptor could have significant internal translational mobility.

Functional Windows.

As mentioned in the *Perspective*, birds have a "functional window" such that a 20-30% change in the intensity of the ambient magnetic field leads to disorientation (50). Fig. S6 illustrates, for a very simple radical pair, how under the right conditions the anisotropic reaction yield of a radical pair reaction can have a strong dependence on the applied magnetic field. The calculations were performed as described in (30) for a radical pair with a single spin-½ nucleus, with an isotropic hyperfine interaction of 1 mT and a very small axial hyperfine anisotropy (20 μT). Fig. S6 *Top*: triplet yield anisotropy plots (the heights of the vertical scale bars correspond to triplet yields of 2%). Fig. S6 *Middle*: The corresponding signal modulation patterns with a field of view of ±31° in the horizontal and vertical directions. Fig. S6 *Bottom*: A measure of the anisotropy of the reaction yield plotted against the field strength.

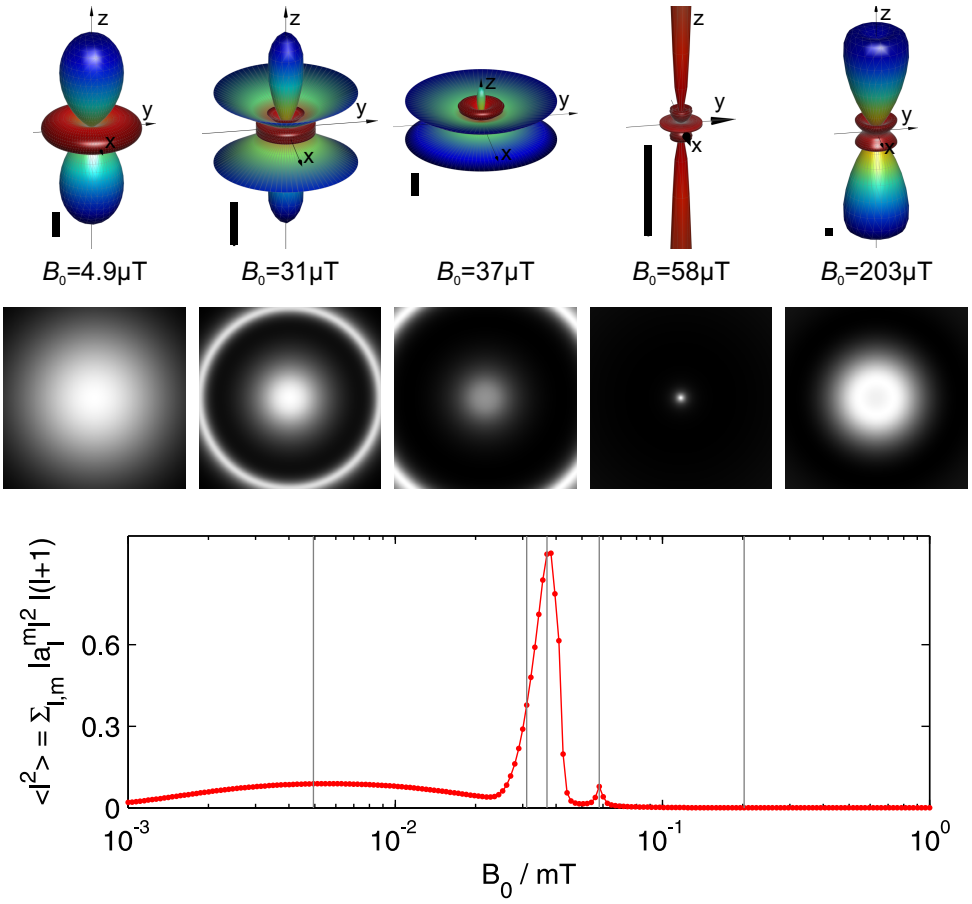

Fig. S6. Reaction yield anisotropies and signal modulation patterns for a simple radical pair subject to applied magnetic fields of various intensities. These calculations indicate a possible origin of the functional window of the avian magnetic compass.

These calculations were performed in a 1-proton radical pair model system with rate constants $k_S^f = 0$; $k_S^b = k_T^f = k = 2\times10^5$ s^{-1} and a hyperfine tensor (in millitesla) of

$$A = \begin{pmatrix} 0.98 & 0 & 0 \\ 0 & 0.98 & 0 \\ 0 & 0 & 1.04 \end{pmatrix}$$

Triplet yield anisotropy calculations and signal modulation plots were made for 200 magnetic field strengths, spread logarithmically between 1 μT and 1 mT. Five illustrative examples of these are shown in the top part of Fig. S6.

In order to quantify the triplet yield anisotropy, we follow the procedure developed in (30, 51) expanding the triplet yield as a sum of spherical harmonics

$$\Phi_{\mathrm{T}}(\theta,\phi) = \sum_{l,m} a_{l,m} Y_{l,m}(\theta,\phi)$$

The lower part of Fig. S6 shows a plot against magnetic field strength of

$$\left\langle l^2 \right\rangle = \sum_{l,m} \left| a_{l,m} \right|^2 l(l+1)$$

This quantity, which is equivalent to the "angular momentum" of a triplet yield anisotropy pattern, is invariant under rotations and quantifies the degree of anisotropy present. It is clear that peaks in this lower graph correspond to different classes of behavior in the triplet yield anisotropy and signal modulation plots shown in the upper parts of the figure. Such analysis is developed in detail in ref. 30.

Flavin Oxidation States.

The structures of the 5 common redox states of the isoalloxazine moiety of flavins: fully oxidized (F), 1-electron reduced ($FH^{\bullet}$ and $F^{\bullet-}$) and fully (2-electron) reduced (FH_2 and FH^-) are given in Fig. S7. The positions of N5 and N10 are shown, following the conventional numbering scheme for flavins (52, 53). The hyperfine tensors of N5 and N10 are large, axial and collinear and may dominate the anisotropy of the response of flavin containing radical pairs to weak magnetic fields (31).

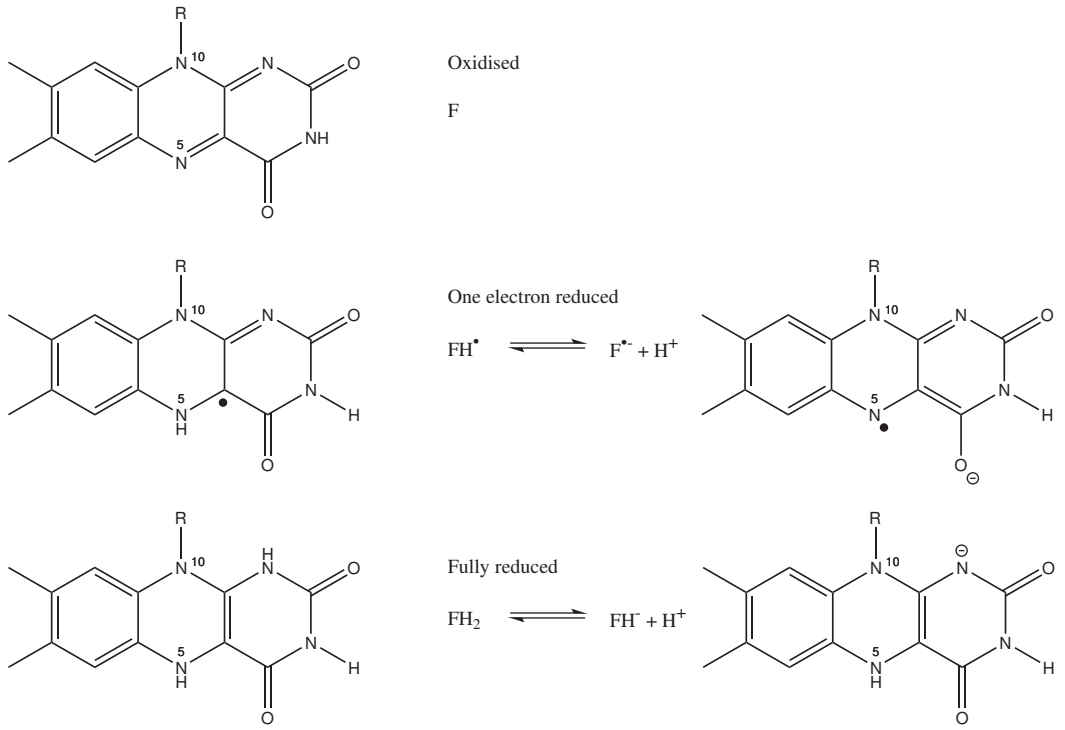

Fig. S7. Structures of the 5 common redox and ionization states of the flavin isoalloxazine moiety.

Cryptochrome Trp-Triad.

The distances between the components of the Trp-triad electron transfer chain in *At*Cry1 (in nanometers), calculated from the X-ray crystal structure of Cry1 from *Arabidopsis thaliana* (54), are shown in Fig. S8. The center of each group (the tricyclic isoalloxazine of the FAD or the indole part of the tryptophan) was determined as the mean of the crystallographic coordinates of all the ring carbon and nitrogen atoms (i.e., 14 atoms for the flavin and 9 for a tryptophan). In each case the edge-to-edge distance is the smallest separation between C or N ring atoms.

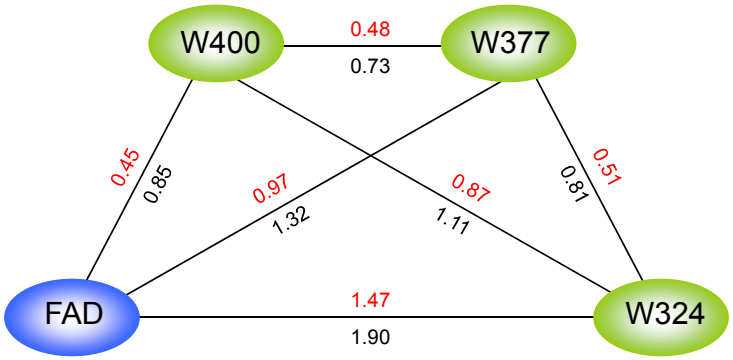

Fig. S8. Distances between the components of the Trp-triad electron transfer chain in *Arabidopsis thaliana* Cry1 (in nanometers). Red, edge-to-edge distances; black, center-to-center distances.

The scheme in Fig. S9 shows a possible cryptochrome photocycle based on Fig. S3. Once again, the amino acid sequence numbers for *At*Cry1 are used. The protonation of the excited state FAD* (55) is not shown explicitly, and the deprotonation and subsequent reduction of the cation radical of the terminal tryptophan ($W324^{\bullet+}$) (56) is omitted. The formation of the [$FADH^{\bullet}$ $W400^{\bullet+}$] and [$FADH^{\bullet}$ $W377^{\bullet+}$] states need not be irreversible. Also, both these radical pairs may undergo back electron transfer to form the ground state, FAD.

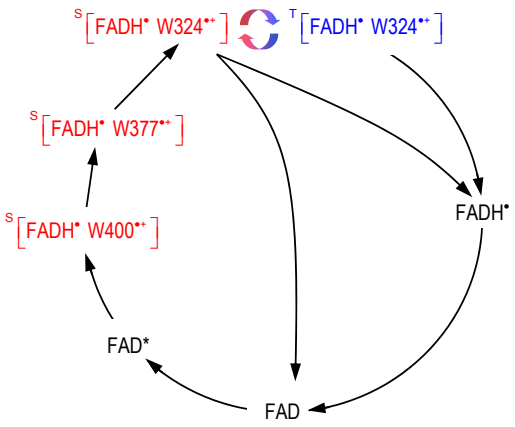

Fig. S9. A possible cryptochrome photocycle, based on Fig. S3.

Alternative Radical Pairs in Cryptochromes.

Flavin-tryptophan (or flavin-tyrosine) radical pairs are not the only potentially magnetically sensitive species that could arise in cryptochromes. Both the semi-and fully reduced forms of flavins are efficiently oxidized by molecular oxygen (57, 58) via reactions that may involve spin-correlated radical pairs or radical-triplet pairs. It is possible to imagine, therefore, that magnetic field-sensitivity comes from the reoxidation of photochemically reduced states of cryptochromes. Although it is far from clear whether either oxygen (a molecular triplet state) or its reduced form (the superoxide radical, $O_2^{\bullet -}$) would satisfy the requirement for slow spin relaxation, such "dark" reactions could conceivably form the basis of a magnetoreceptor. A hypothetical reaction scheme involving a $FADH^{\bullet}$-superoxide radical triplet pair is shown in Fig. S10. It is assumed that the FADH radical is formed photochemically by electron transfer via the Trp-triad and that molecular oxygen is responsible for regeneration of the fully oxidized state of the protein via the dark reactions shown. The radical triplet pair $\left[FADH^{\bullet}\ O_2^{\bullet -}\right]$ can be formed in both doublet and quartet states but can only react via the doublet state.

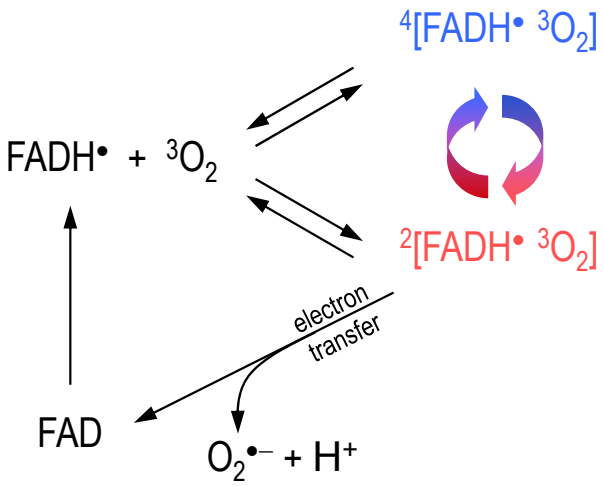

Fig. S10. Hypothetical reaction scheme, involving a $FADH^\bullet$-superoxide radical triplet pair, that could account for magnetic sensitivity in cryptochrome.

An attractive aspect of this idea is that neither O_2 nor $O_2^{\bullet-}$ has hyperfine interactions, at least when they are not hydrogen bonded. Simulations suggest that radical pairs in which the magnetic nuclei are highly asymmetrically distributed between the 2 radicals tend to exhibit stronger magnetic field effects than those which have the hyperfine interactions more uniformly spread and that such radical pairs may be especially sensitive to radio frequency fields at the EPR frequency (1.4 MHz in a 50-μT field) (2, 30, 59). As mentioned in the *Perspective*, a radical pair in which one radical has no hyperfine interactions is suggested by behavioral experiments on birds exposed to radio frequency fields (60, 61).

A Comment on the Radical Pair Mechanism as a Source of Biological Magnetic Field Effects.

A common objection to any proposal that weak (<100 μT) magnetic fields may affect biological systems is that the required interactions are dwarfed by intrinsic, naturally occurring "background" magnetic fields. In the radical pair context it is indeed true that the local magnetic fields produced by the nuclear spins of such ubiquitous isotopes as ^1H, ^{14}N and ^{31}P are frequently much larger than 100 μT. But far from dominating the effect of a weak applied field, isotropic hyperfine interactions fields are, paradoxically, crucial to its existence, as discussed in the *Perspective*.

Another, closely related, source of local magnetic fields that are also essential for compass action are the anisotropic parts of the hyperfine interactions which become time-dependent through their modulation by molecular motions. The result of this "magnetic noise" is spin relaxation, which as argued in the Perspective can be slow enough that it should not interfere too much with the spin dynamics. Other possible sources of magnetic interference are paramagnetic molecules (other than the radical pair itself) and magnetic particles, e.g., magnetite (62). The fields produced by the former, though potentially much stronger than hyperfine interactions, are short range and, like anisotropic hyperfine couplings, likely to produce at most small contributions to spin relaxation rates. Magnetite and other magnetic particles are not sufficiently widespread in biological tissue that they need be considered in this context.

1. Solov'yov IA, Chandler DE, Schulten K (2007) Magnetic field effects in *Arabidopsis thaliana* cryptochrome-1. *Biophys J* 92:2711-2726.

2. Efimova O, Hore PJ (2008) Role of exchange and dipolar interactions in the radical pair model of the avian magnetic compass. *Biophys J* 94:1565-1574.

3. Henbest KB*, et al.* (2008) Magnetic-field effect on the photoactivation reaction of *Escherichia coli* DNA photolyase. *Proc Natl Acad Sci USA* 105:14395-14399.

4. Harkins TT, Grissom CB (1994) Magnetic-field effects on B-12 ethanolamine ammonia-lyase - evidence for a radical mechanism. *Science* 263:958-960.

5. Harkins TT, Grissom CB (1995) The magnetic-field dependent step in B_{12} ethanolamine ammonia-lyase is radical-pair recombination. *J Am Chem Soc* 117:566-567.

6. Canfield JM, Belford RL, Debrunner PG (1996) Calculations of Earth-strength steady and oscillating magnetic field effects in coenzyme B-12 radical pair systems. *Mol Phys* 89:889-930.

7. Taraban MB, Leshina TV, Anderson MA, Grissom CB (1997) Magnetic field dependence of electron transfer and the role of electron spin in heme enzymes: Horseradish peroxidase. *J Am Chem Soc* 119:5768-5769.

8. Afanasyeva MS*, et al.* (2006) Elementary steps of enzymatic oxidation of nifedipine catalyzed by horseradish peroxidase. *J Phys Chem B* 110:21232-21237.

9. Afanasyeva MS, Taraban MB, Purtov PA, Leshina TV, Grissom CB (2006) Magnetic spin effects in enzymatic reactions: Radical oxidation of NADH by horseradish peroxidase. *J Am Chem Soc* 128:8651-8658.

10. Chalkias NG, Kahawong P, Giannelis EP (2008) Activity increase of horseradish peroxidase in the presence of magnetic particles. *J Am Chem Soc* 130:2910-2911.

11. Møller AC, Lunding A, Olsen LF (2000) Further studies of the effect of magnetic fields on the oscillating peroxidase-oxidase reaction. *Phys Chem Chem Phys* 2:3443-3446.

12. Møller AC, Olsen LF (1999) Effect of magnetic fields on an oscillating enzyme reaction. *J Am Chem Soc* 121:6351-6354.

13. Møller AC, Olsen LF (2000) Perturbations of simple oscillations and complex dynamics in the peroxidase-oxidase reaction using magnetic fields. *J Phys Chem B* 104:140-146.

14. Carson JJL, Walleczek J (2003) Response of the peroxidase-oxidase oscillator to light is controlled by MB^+-NADH photochemistry. *J Phys Chem B* 107:8637-8642.

15. Jones AR, Hay S, Woodward JR, Scrutton NS (2007) Magnetic field effect studies indicate reduced geminate recombination of the radical pair in substrate-bound adenosylcobalamin-dependent ethanolamine ammonia lyase. *J Am Chem Soc* 129:15718-15727.

16. Jones AR, Scrutton NS, Woodward JR (2006) Magnetic field effects and radical pair mechanisms in enzymes: A reappraisal of the horseradish peroxidase system. *J Am Chem Soc* 128:8408-8409.

17. Seagle BLL, Gasyna EM, Mieler WF, Norris JR (2006) Photoprotection of human retinal pigment epithelium cells against blue light-induced apoptosis by melanin free radicals from *Sepia officinalis*. *Proc Natl Acad Sci USA* 103:16644-16648.

18. Richter G*, et al.* (2005) Photochemically induced dynamic nuclear polarization in a C450A mutant of the LOV2 domain of the *Avena sativa* blue-light receptor phototropin. *J Am Chem Soc* 127:17245-17252.

19. Eisenreich W, Joshi M, Weber S, Bacher A, Fischer M (2008) Natural abundance solution C-13 NMR studies of a phototropin with photoinduced polarization. *J Am Chem Soc* 130:13544-13545.

20. Buchachenko AL, Kouznetsov DA, Breslavskaya NN, Orlova MA (2008) Magnesium isotope effects in enzymatic phosphorylation. *J Phys Chem B* 112:2548-2556.

21. Buchachenko AL, Kouznetsov DA, Orlova MA, Markarian AA (2005) Magnetic isotope effect of magnesium in phosphoglycerate kinase phosphorylation. *Proc Natl Acad Sci USA* 102:10793-10796.

22. Buchachenko AL, Kouznetsov DA, Shishkov AV (2004) Spin biochemistry: Magnetic isotope effect in the reaction of creatine kinase with CH_3HgCl. *J Phys Chem A* 108:707-710.

23. Kobori Y, Norris JR (2006) 1D radical motion in protein pocket: Proton-coupled electron transfer in human serum albumin. *J Am Chem Soc* 128:4-5.

24. Miura T, Maeda K, Arai T (2003) Effect of coulomb interaction on the dynamics of the radical pair in the system of flavin mononucleotide and hen egg-white lysozyme (HEWL) studied by a magnetic field effect. *J Phys Chem B* 107:6474-6478.

25. Mok KH, Hore PJ (2004) Photo-CIDNP NMR methods for studying protein folding. *Methods* 34:75-87.

26. Mok KH*, et al.* (2007) A pre-existing hydrophobic collapse in the unfolded state of an ultrafast folding protein. *Nature* 447:106-109.

27. Hore PJ, Broadhurst RW (1993) Photo-CIDNP of biopolymers. *Prog Nucl Magn Reson Spectrosc* 25:345-402.

28. Kaptein R, Dijkstra K, Nicolay K (1978) Laser photo-CIDNP as a surface probe for proteins in solution. *Nature* 274:293-294.

29. Timmel CR, Till U, Brocklehurst B, McLauchlan KA, Hore PJ (1998) Effects of weak magnetic fields on free radical recombination reactions. *Mol Phys* 95:71-89.

30. Rodgers CT (2007) D. Phil. thesis. University of Oxford

31. Cintolesi F, Ritz T, Kay CWM, Timmel CR, Hore PJ (2003) Anisotropic recombination of an immobilized photoinduced radical pair in a 50-μT magnetic field: a model avian photomagnetoreceptor. *Chem Phys* 294:385-399.

32. Ritz T, Adem S, Schulten K (2000) A model for photoreceptor-based magnetoreception in birds. *Biophys J* 78:707-718.

33. Moser CC, Dutton PL (1992) Engineering protein-structure for electron-transfer function in photosynthetic reaction centers. *Biochim Biophys Acta* 1101:171-176.

34. Weiss EA*, et al.* (2004) Making a molecular wire: Charge and spin transport through para-phenylene oligomers. *J Am Chem Soc* 126:5577-5584.

35. Weiss EA, Tauber MJ, Ratner MA, Wasielewski MR (2005) Electron spin dynamics as a probe of molecular dynamics: Temperature-dependent magnetic field effects on charge recombination within a covalent radical ion pair. *J Am Chem Soc* 127:6052-6061.

36. Verhoeven JW (2006) On the role of spin correlation in the formation, decay, and detection of long-lived, intramolecular charge-transfer states. *J Photochem Photobiol C* 7:40-60.

37. Dittrich M, Freddolino PL, Schulten K (2005) When light falls in LOV: A quantum mechanical/molecular mechanical study of photoexcitation in Phot-LOV1 of *Chlamydomonas reinhardtii*. *J Phys Chem B* 109:13006-13013.

38. Kennis JTM, Groot ML (2007) Ultrafast spectroscopy of biological photoreceptors. *Curr Opin Struct Biol* 17:623-630.

39. Schleicher E*, et al.* (2004) On the reaction mechanism of adduct formation in LOV domains of the plant blue-light receptor phototropin. *J Am Chem Soc* 126:11067-11076.

40. Gauden M*, et al.* (2006) Hydrogen-bond switching through a radical pair mechanism in a flavin-binding photoreceptor. *Proc Natl Acad Sci USA* 103:10895-10900.

41. Weber S (2005) Light-driven enzymatic catalysis of DNA repair: a review of recent biophysical studies on photolyase. *Biochim Biophys Acta* 1707:1-23.

42. Zech SG*, et al.* (1997) Pulsed EPR measurement of the distance between $P_{680}^{+\bullet}$ and $Q_A^{-\bullet}$ in photosystem II. *FEBS Lett* 414:454-456.

43. Zech SG, Kurreck J, Renger G, Lubitz W, Bittl R (1999) Determination of the distance between $Y_Z^{ox\bullet}$ and $Q_A^{-\bullet}$ in photosystem II by pulsed EPR spectroscopy on light-induced radical pairs. *FEBS Lett* 442:79-82.

44. Stehlik D, Bock CH, Petersen J (1989) Anisotropic electron-spin polarization of correlated spin pairs in photosynthetic reaction centers. *J Phys Chem* 93:1612-1619.

45. Bertini I, Luchinat C (1986) *NMR of paramagnetic molecules in biological systems* (Benjamin/Cummings, Menlo Park, California).

46. Bhattacharjee B, Das R (2007) Involvement of triplet state in the photodissociation of hydrogen peroxide: experimental evidence from time-resolved EPR study. *Mol Phys* 105:1053-1057.

47. Forbes MDE*, et al.* (2007) On the electron spin polarization observed in TREPR experiments involving hydroxyl and sulfate radicals. *Mol Phys* 105:2127-2136.

48. van den Brink JS, Hermolle TEP, Gast P, Hore PJ, Hoff AJ (1996) Electron spin polarization of the oxidized primary electron donor in reaction centers of photosynthetic purple bacteria. *J Phys Chem* 100:2430-2437.

49. Eveson RW, Timmel CR, Brocklehurst B, Hore PJ, McLauchlan KA (2000) The effects of weak magnetic fields on radical recombination reactions in micelles. *Int J Radiat Biol* 76:1509-1522.

50. Wiltschko R, Wiltschko W (1995) *Magnetic orientation in animals* (Springer Verlag, Berlin).

51. Maeda K*, et al.* (2008) Chemical compass model of avian magnetoreception. *Nature* 453:387-309.

52. Heelis PF (1991) in *The Chemistry and Biochemistry of Flavoenzymes* (CRC Press, Boca Raton), pp 171-193.

53. Müller F (1991) in *The Chemistry and Biochemistry of Flavoenzymes* (CRC Press, Boca Raton), pp 1-71.

54. Brautigam CA*, et al.* (2004) Structure of the photolyase-like domain of cryptochrome 1 from *Arabidopsis thaliana*. *Proc Natl Acad Sci USA* 101:12142-12147.

55. Kottke T, Batschauer A, Ahmad M, Heberle J (2006) Blue-light-induced changes in *Arabidopsis* cryptochrome 1 probed by FTIR difference spectroscopy. *Biochemistry* 45:2472-2479.

56. Byrdin M*, et al.* (2004) Intraprotein electron transfer and proton dynamics during photoactivation of DNA photolyase from *E. coli*: review and new insights from an "inverse" deuterium isotope effect. *Biochim Biophys Acta* 1655:64-70.

57. Műller F (1987) Flavin Radicals - Chemistry and Biochemistry. *Free Radical Biol Med* 3:215-230.

58. Prabhakar R, Siegbahn PEM, Minaev BF, Agren H (2002) Activation of triplet dioxygen by glucose oxidase: Spin-orbit coupling in the superoxide ion. *J Phys Chem B* 106:3742-3750.

59. Rodgers CT, Norman SA, Henbest KB, Timmel CR, Hore PJ (2007) Determination of radical re-encounter probability distributions from magnetic field effects on reaction yields. *J Am Chem Soc* 129:6746-6755.

60. Ritz T, Thalau P, Phillips JB, Wiltschko R, Wiltschko W (2004) Resonance effects indicate a radical-pair mechanism for avian magnetic compass. *Nature* 429:177-180.

61. Ritz T*, et al.* (2008) Magnetic compass of birds is based on a molecule with optimal directional sensitivity. *Biophys J* in press.

62. Binhi V (2008) Do naturally occurring magnetic nanoparticles in the human body mediate increased risk of childhood leukaemia with EMF exposure? *Int J Radiat Biol* 84:569-579.